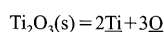


## Fundamentals of High Temperature Processes

Temperature Dependence of Ti Deoxidation Equilibria of Liquid Iron in Coexistence with 'Ti<sub>3</sub>O<sub>5</sub>' and Ti<sub>2</sub>O<sub>3</sub>W.-Y. CHA *et al.*

The equilibrium relation between Ti and O in liquid Fe has been measured only at 1873 K on the condition of various kinds of titanium oxides saturation in our previous paper. The present work deals with the equilibrium between Ti and O in liquid Fe saturated with 'Ti<sub>3</sub>O<sub>5</sub>' and Ti<sub>2</sub>O<sub>3</sub> at 1823 K and 1923 K for full understanding temperature dependence. Also, equilibrium phase changes of titanium oxides with various Ti contents in molten Fe have been identified as the equilibrium titanium oxides with electron backscatter diffraction (EBSD) pattern analysis technique. The present results have been thermodynamically evaluated combining with previous results on the various thermodynamic values as a function of temperature.

The equilibrium constants and the interaction parameters of Wagner's formalism were given as a function of temperature in the present work as follows.

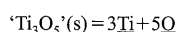


$$\log K_{\text{Ti}_2\text{O}_3} = -42940/T + 12.94,$$

$$(1823\text{ K} < T < 1923\text{ K})$$

$$\begin{cases} -10.61, 0.28 < \text{mass\%Ti} < 4.89, \text{ at } 1823\text{ K} \\ -9.99, 0.40 < \text{mass\%Ti} < 6.22, \text{ at } 1873\text{ K} \\ -9.39, 0.52 < \text{mass\%Ti} < 2.79, \text{ at } 1923\text{ K} \end{cases}$$

$$e_{\text{O}}^{\text{Ti}} = -701/T + 0.0344, \quad (1823\text{ K} < T < 1923\text{ K})$$



$$\log K_{\text{'Ti}_3\text{O}_5\text{'}} = -68280/T + 19.95,$$

$$(1823\text{ K} < T < 1923\text{ K})$$

$$\begin{cases} -17.50, 0.01 < \text{mass\%Ti} < 0.28, \text{ at } 1823\text{ K} \\ -16.52, 0.006 < \text{mass\%Ti} < 0.40, \text{ at } 1873\text{ K} \\ -15.56, 0.0045 < \text{mass\%Ti} < 0.52, \text{ at } 1923\text{ K} \end{cases}$$

$$e_{\text{O}}^{\text{Ti}} = -701/T + 0.0344, \quad (1823\text{ K} < T < 1923\text{ K})$$

The Henry constant of Ti in liquid Fe was estimated as a function of temperature.

$$\ln \gamma_{\text{Ti}}^{\circ} = -20890/T + 6.228, \\ (1823\text{ K} < T < 1923\text{ K})$$

The self-interaction parameter of Ti in liquid Fe was obtained as a function of temperature.

$$e_{\text{Ti}}^{\text{Ti}} = 212/T - 0.0640, \quad (1823\text{ K} < T < 1923\text{ K})$$

The interaction parameters of Redlich-Kister type polynomial for molten Fe-Ti-O alloy were given as the following values in the present work.

$${}^{\circ}\Omega_{\text{Fe-Ti}} = -173600 + 51.76T/J, \\ (1823\text{ K} < T < 1923\text{ K})$$

$${}^{\circ}\Omega_{\text{Ti-O}} = -1189000 + 82.00T/J, \\ (1823\text{ K} < T < 1923\text{ K})$$

The estimated results based on Wagner's formalism as well as Darken's quadratic formalism with Redlich-Kister type polynomials agreed well with the experimental results at 1823 to 1923 K.

(cf. ISIJ Int., 48 (2008), 729)

The Influence of Al<sub>2</sub>O<sub>3</sub>/SiO<sub>2</sub> Ratio on the Viscosity of Mold FluxesZ. ZHANG *et al.*

The present paper investigates how the  $X_{\text{Al}_2\text{O}_3}/X_{\text{SiO}_2}$  ratio in mold slag compositions in a range between 0.06 and 2.14 influences the viscosity of the melt. The objective was to study the variation in viscosity of mould slags if they get enriched in Al<sub>2</sub>O<sub>3</sub> as a result of reactions during continuous casting with high Al containing steel melts for manufacturing TRIP steels.

The viscosity was found to increase with increasing  $X_{\text{Al}_2\text{O}_3}/X_{\text{SiO}_2}$  ratio but a change in the degree of increase was noted at a ratio of 0.57. The effect of increasing temperature was investigated and it was shown that viscosity decreased, as expected, with increasing temperature. An available model in literature for predicting the mold-slag viscosity was empirically modified to account for high Al<sub>2</sub>O<sub>3</sub> contents investigated in this study.

Increasing  $X_{\text{Al}_2\text{O}_3}/X_{\text{SiO}_2}$  did not appear to influence the vaporization loss of F but increasing the ratio did influence crystallization by promoting the precipitation of CaF<sub>2</sub> during slow cooling of samples with a high  $X_{\text{Al}_2\text{O}_3}/X_{\text{SiO}_2}$  ratio (0.84 and 2.14).

(cf. ISIJ Int., 48 (2008), 739)

## Simulation Test for Crystallization of Inclusions in Semi-killed Steels during Heat Treatment Prior to Hot Rolling

C. ZHAO *et al.*

The SHTT (Single Hot Thermocouple Technique) has been used to determine the crystallization behavior of a composition of the CaO-Al<sub>2</sub>O<sub>3</sub>-SiO<sub>2</sub> system, representative of inclusions in semi-killed steels. XRD and SEM have been employed, respectively, to detect the crystalline phases and to analyze the morphology, quantity and properties of crystals. The same composition has also been studied by quenching the oxides in iron crucibles, a method which had been proven reliable to simulate the actual behavior of inclusions in steel samples during heat treatment prior to hot rolling. The TTT diagrams obtained by using the above two techniques are almost identical. The observed crystalline phases for this composition are gehlenite (2CaO·Al<sub>2</sub>O<sub>3</sub>·SiO<sub>2</sub>) and anorthite (CaO·Al<sub>2</sub>O<sub>3</sub>·2SiO<sub>2</sub>). The TTT diagram from SHTT gives the nose position of gehlenite and anorthite of, respectively, 1200 s at 1200°C and 4800 s at 1300°C. Thus, the Hot Thermocouple Technique (DHTT or SHTT), already largely used to study the crystallization behavior of CC mold slags is shown to be suitable to simulate the crystallization behavior of inclusions with much higher SiO<sub>2</sub> contents.

(cf. ISIJ Int., 48 (2008), 747)

## Magnesium Deoxidation Equilibrium of Molten Fe-Ni Alloy Expressed by Quadratic Formalism and Redlich-Kister Type Polynomial

M. YONEMOTO *et al.*

Magnesium deoxidation equilibrium of molten Fe-Ni alloy was determined by a chemical equilibrium method at temperature of 1873 to 1973 K. Ex-

treme care was taken for oxygen analysis of the samples. Numerical analysis on Mg deoxidation of molten Fe-Ni alloy has been carried out by utilizing the model based on Darken's quadratic formalism and Redlich-Kister type polynomial.

(cf. ISIJ Int., 48 (2008), 755)

## Corrosion Mechanism of Commercial MgO-C Refractories in Contact with Different Gas Atmospheres

S. JANSSON *et al.*

Corrosion of MgO-C refractories in different gas atmospheres consisting of air, Ar, CO or Ar/CO was studied in laboratory experiments. In total, 103 experiments were carried out in the temperature range 1173 to 1773 K and for holding times between 2 to 120 min. The reaction rate of the MgO-C material was determined from measurements of the weight loss of the samples. The results showed that the refractory weight loss increased with an increased temperature or an increased holding time. The thermodynamic conditions and the experimental results showed that magnesium gas and carbon monoxide gas should form during ladle refining of steel when the refractory material consists of MgO-C. It was suggested that the reaction rate is directly dependent on the oxygen potential in the ambient atmosphere.

(cf. ISIJ Int., 48 (2008), 760)

## Ironmaking

## Influence of Pellet Size on Quality and Microstructure of Iron Ore Pellets

S. DWARAPUDI *et al.*

During the induration of pellets, temperature and oxygen partial pressure influence the formation of different phases and microstructure. With increasing the pellet size, these thermo-chemical conditions vary across its cross section. The time difference between the oxidation of the pellet surface and the core increases with increasing pellet size, i.e. the oxidation takes place under different conditions resulting in different phases and microstructure. In this study commercial pellets of different sizes (8-16 mm) were studied for their physical, mechanical and metallurgical properties. Pellets in the size range of 10-12.5 mm showed superior properties. Electron and optical micro structural studies with image analysis revealed that hematite content, pore density, amount and distribution of silicate melt of different sized pellets are different and distinctly affect the pellet quality. SEM-EDX analysis and X-ray mapping techniques revealed that Mg has a specific distribution pattern across the cross section of the pellet.

(cf. ISIJ Int., 48 (2008), 768)

## Three-dimensional Modelling of Coal Combustion in Blast Furnace

Y. SHEN *et al.*

Pulverized coal injection technology is widely used in blast furnace ironmaking due to economic, operational and environmental benefits. High burnout within the tuyere and raceway is required for high coal injection rate operation. In order to analyze the flow and

combustion in the tuyere and raceway more accurately and reliably, a three-dimensional model of coal combustion is developed. This model is validated against the measurements from two pilot scale test rigs in terms of gas species composition and coal burnout. The gas-solid flow and coal combustion are simulated and analysed. The results indicate that compared to our previous model, the present model is able to provide more complete gas species distributions and better describe the evolutions of coal particles. It is more sensitive to various parameters and hence more robust in examining various blast furnace operations.

(cf. *ISIJ Int.*, **48** (2008), 777)

## Steelmaking

### Modelling of Inclusion Motion and Flow Patterns in Swirling Flow Tundishes with Symmetrical and Asymmetrical Structures

*Q. HOU et al.*

Swirling flow tundish (SFT) has recently been developed as a new type of tundish. Its key mechanism is forming swirling flow to enhance inclusion removal from steel for high quality slab casting. This is achieved by guiding the liquid steel into the tundish through the tangential inlet of a cylindrical swirling chamber (SC). This can restrain and alleviate the turbulence of the impact zone. SC has been settled into two types of tundishes—originally symmetrical and asymmetrical. To understand the fundamentals, physical and mathematical modellings of this new process have been conducted in this work. Physical modellings are carried out with the utilization of an asymmetrical one-strand 1:2.5 and a symmetrical two-strand 1:3 scale models. The internal flow is measured by digital particle image velocimetry (DPIV). Numerical modelling is carried out in line with the physical modelling to examine the details of the flow patterns and rotational effect caused by the SC. The trajectories of non-metallic inclusion particles are also studied by discrete phase model (DPM) within the commercial CFD package environment, FLUENT. The mathematical model proposed is validated by comparing the predicted and measured residence time distribution and velocity fields. The results show that both originally symmetrical and asymmetrical flow fields have been changed to asymmetrical ones after setting SC into it. And the results show that the flow is slower behind the dam and weir. Examinations of the trajectories of inclusion particles suggest that the inclusion removal capacity of the SFT is higher than the tundish with a turbulence inhibitor (TI). From the separation ratio results, it can be seen that SFT has higher ability to remove small inclusion particles than a tundish with TI, which is of great significance especially for production of high-quality steel.

(cf. *ISIJ Int.*, **48** (2008), 787)

### Influence of Bottom Tuyere Configuration on Bath Stirring in a Top and Bottom Combined Blown Converter

*Z. LAI et al.*

Influence of bottom tuyere configuration on bath stirring in top and bottom combined blown convert-

er was investigated with physical modeling experiments by measuring mixing time of bath. The results showed that asymmetric bottom tuyere configurations have shorter bath mixing time than symmetric bottom tuyere configurations due to their better bath stirring effect. Bath oscillation in converters with too high top gas flow rates would deteriorate the bath stirring and prolong the bath mixing time in the case of asymmetric bottom tuyere configurations. The industrial application data indicated that the converter with asymmetric bottom tuyere arrangement showed better metallurgical results at tapping. Average tapping  $[O]_e$  decreased by 160 ppm and average tapping  $[C]_e \times [O]_e$  reduced from 0.0031 to 0.0025. Average tapping (T.Fe) $_e$  content in slag decreased by 2.21%, while average tapping  $[Mn]_e$  increased by 0.029%.

(cf. *ISIJ Int.*, **48** (2008), 793)

## Instrumentation, Control and System Engineering

### Modeling and Feed-forward Velocity Compensation of Multi-span Web Transport Systems with Thermal and Gravity Effects

*G. Y. KIM et al.*

A new mathematical model of a web transport system (WTS) in a continuous annealing process (CAP) is proposed. In general, temperature and gravity effects influence the web of a vertical WTS in a CAP. However, these effects are not systematically considered in the conventional mathematical model of a WTS. Disregard for these effects causes a low quality of webs in the CAP. Therefore, in order to improve the quality of webs, a precise web tension control is required based on a mathematical model with thermal and gravity effects. Thus, the mathematical model with thermal and gravity effects in the CAP was established in this paper. In addition, the feed-forward velocity compensator for the web tension control system was suggested, which was based on the proposed mathematical model with thermal and gravity effects. In order to evaluate the validity of the proposed mathematical model for a vertical WTS and the proposed web tension control system in a CAP, computer simulations that considered thermal and gravity effects were executed and an experiment was implemented.

(cf. *ISIJ Int.*, **48** (2008), 799)

## Welding and Joining

### Effects of Heat Input and Martensite on HAZ Softening in Laser Welding of Dual Phase Steels

*M. XIA et al.*

Laser welds were made in three dual-phase (DP) alloys with ultimate tensile strengths ranging from 450–980 MPa and varying microstructures to investigate effects of heat input on heat affected zone (HAZ) softening. To compare the total heat transferred into the HAZ of all the welds, heat input was normalized using the Rosenthal Equation. It was found that HAZ softening experienced in a DP steel was a function of both martensite content and heat input. Maximum HAZ softening was proportional to

the martensite content, and the heat input controlled the completion of softening. Material softening was normalized by martensite content, which showed that the contribution of martensite to material hardness from the three materials is the same; however the materials had different transformation kinetics.

(cf. *ISIJ Int.*, **48** (2008), 809)

## Transformations and Microstructures

### Microstructures and Properties of High-strength Alloys Severely Deformed by Machining

*M. TANAKA et al.*

Microstructures and properties were examined on the chip specimens severely deformed to a given shear strain ( $\gamma$ ) by machining in the high-strength Ni-base Inconel X-750 alloy and 6061-T6 aluminum alloy. Chip specimens have a deformation structure principally composed of elongated grains (for example, a few  $\mu\text{m}$  to about 100  $\mu\text{m}$  in length and about 1  $\mu\text{m}$  to a few tens  $\mu\text{m}$  in width for the chip specimen of  $\gamma \approx 3$  of the Inconel X-750 alloy). Many subgrains separated by small or medium angle grain boundaries (misorientation,  $\theta < 15^\circ$ ) were also observed within relatively large grains. In the case where detailed analysis by FESEM/EBSP was possible, the fraction of large angle grain boundaries ( $\theta \geq 15^\circ$ ) and that of medium angle grain boundaries ( $5^\circ \leq \theta < 15^\circ$ ) were relatively small, and most of grain boundaries were small grain boundaries ( $1^\circ \leq \theta < 5^\circ$ ) in the chip specimens of both alloys. Internal friction of the chip specimen was much larger than that of the original material. Large internal friction of the chip specimens was principally attributed to many cracks formed during machining. The hardness of chip specimens largely increased with increasing shear strain imposed by machining in the Inconel X-750 alloy, although the increase of hardness with shear strain was not so large in the 6061-T6 alloy.

(cf. *ISIJ Int.*, **48** (2008), 815)

### Effects of Aluminum on Delayed Fracture Properties of Ultra High Strength Low Alloy TRIP-aided Steels

*T. HOJO et al.*

To improve the delayed fracture strength of ultra high-strength low alloy TRIP-aided steels with bainitic ferrite matrix (TBF steels), the effects of aluminum content on hydrogen absorption behavior and delayed fracture properties of 0.2%C–0.2–1.5%Si–1.5%Mn TBF steel were investigated. When aluminum was added to the TBF steel, the diffusible hydrogen increased. It was expected that the hydrogen was charged not only in retained austenite films but also on lath boundary. Delayed fracture strength of TBF steels containing aluminum were significantly increased, compared with conventional TBF steel. This was mainly caused by (1) suppression of the stress-assisted martensite transformation resulting from the stabilized or carbon-enriched retained austenite, (2) hydrogen trapping to refined interlath retained austenite films and lath boundary, and (3) relaxation of localized stress concentration by TRIP effect of the retained austenite.

(cf. *ISIJ Int.*, **48** (2008), 824)

### Serial Sectioning and 3D-reconstruction of Ferrite Allotriomorphs Nucleated at Grain Boundary Faces in an Fe–C–Mn Alloy

L. CHENG *et al.*

Three-dimensional morphology of ferrite allotriomorphs nucleated at grain boundary faces in an Fe–0.09%C–1.48%Mn alloy was revealed by means of serial sectioning in conjunction with computer-aided three-dimensional reconstruction techniques. Ferrite allotriomorphs formed at grain boundary faces appeared to be oblate ellipsoids on usual two-dimensional planar sections. Three-dimensional reconstruction shows that they were large in one dimension, specifically in the depth direction of specimens in this study, some of them being approximately prolate ellipsoids rather than an equiaxed pancake shape as usually assumed.

(cf. *ISIJ Int.*, **48** (2008), 830)

### Thermodynamic Analysis of the Fe–Nb–B Ternary System

K. YOSHITOMI *et al.*

A thermodynamic analysis of the Fe–Nb–B ternary system has been carried out by estimating the unknown thermodynamic properties of various borides and solid solutions with using a first-principles method. The calculations showed that, at least in the ground state, the solid solution, in which the B atoms substitute for the Fe atoms, was more probable than that where the B atoms dissolved in the octahedral interstitial sites. Furthermore, the calculated values for the binary borides in the Fe–B and Nb–B systems were in reasonable agreement with those found by experiment. The thermodynamic properties such as formation enthalpies for the FeNbB and Nb<sub>3</sub>B<sub>2</sub> phases were also determined for ternary borides. The thermodynamic functions determined using these theoretical values, as well as the available experimental information on the phase boundaries, successfully revealed the phase equilibria in the Fe–Nb–B ternary system over the entire composition and temperature ranges.

(cf. *ISIJ Int.*, **48** (2008), 835)

### Effect of Mn on Solubility of Ti-sulfide and Ti-carbosulfide in Ultra-low C Steels

N. MIZUT *et al.*

To clarify the thermodynamic stability of Ti<sub>4</sub>C<sub>2</sub>S<sub>2</sub> and TiS in ULC Ti-added IF steels, extraction by potentiostatic electrolysis method and chemical analysis were conducted with ULC Ti-added IF steels containing various amounts of Mn and heated at various temperatures. As the results, the solubilities of Ti<sub>4</sub>C<sub>2</sub>S<sub>2</sub> and TiS increased with an increase in

Mn content. Ti<sub>4</sub>C<sub>2</sub>S<sub>2</sub> was more stable than TiS between 950 and 1250°C. Following solubility products were obtained.

$$\log[\text{Ti}] \cdot [\text{C}]^{0.5} \cdot [\text{S}]^{0.5} = 0.392 - 7004/T - (4.783 - 7401/T) \cdot [\text{Mn}]$$

$$\log[\text{Ti}]^{2/3} \cdot [\text{S}] = -0.021 - 5847/T - (3.360 - 5195/T) \cdot [\text{Mn}]$$

(cf. *ISIJ Int.*, **48** (2008), 845)

### Mechanical Properties

#### Investigation on Mechanical Behaviors for Bolted Connections in Carbon Steel and in Stainless Steel Using FEM

T.S. KIM *et al.*

A finite element (FE) analysis with three-dimensional solid elements has been performed for estimating the structural behaviors of single shear bolted connections fabricated with cold-formed austenitic stainless steel by utilizing the existing test data for calibration. Failure and curling (out-of-plane deformation perpendicular to the direction of loading) criteria were proposed. Therefore, the failure mode and ultimate strength, predicted by FE analysis method, showed good agreements with those of experimental results. In this study, FE analyses for 10 test specimens fabricated with cold-formed carbon steel as well as stainless steel including failure mode of bolt shear fracture are carried out and the validity of numerical prediction for ultimate behaviors in cold-formed carbon steel bolted connections is also verified, based on the applicability of FE method for predicting the mechanical behaviors of bolted connections in cold-formed stainless steel. It is known from the coupon test results of steel materials that austenitic stainless (SUS304) steel has a higher tensile strength of material due to the effect of strength enhancements (considerable strain hardening) by means of cold-working process and much lower yield stress when compared to carbon steel. The influence of curling on the strength reduction of bolted connections is estimated quantitatively. In addition, characteristics of mechanical behaviors and the influence of curling in bolted connections between two different steel materials are compared through detailed investigation of FE analysis results.

(cf. *ISIJ Int.*, **48** (2008), 851)

#### Factors Inducing Intergranular Fracture in Nickel-free High Nitrogen Austenitic Stainless Steel Produced by Solution Nitriding

T. TSUCHIYAMA *et al.*

Fe–25mass%Cr–1.1mass%N alloys with different impurity content were produced by solution nitrid-

ing and then subjected to tensile tests at ambient temperature. Yield strength and tensile strength of the alloys are much higher than those of conventional austenitic stainless steels, but the brittle intergranular fracture is caused during uniform deformation without local elongation. It was confirmed that the intergranular fracture takes place at high angle random boundary and that the grain boundary segregation of impurities significantly promotes intergranular fracture. Deformation-induced martensite did not concern the intergranular fracture. In addition, it was suggested that marked stress concentration is caused at grain boundary by the piled-up dislocations in planar array and it would be one of the important factors inducing intergranular fracture.

(cf. *ISIJ Int.*, **48** (2008), 861)

### Social and Environmental Engineering

#### Application of *Terminalia chebula* for Removal of Hexavalent Chromium in Chromite Concentrates

G. KAPURE *et al.*

Hexavalent chromium, Cr(VI) presence in chromite concentrate is a concern due to its environmental unfriendly and carcinogenic nature. Chromite concentrates typically contain Cr(VI) in the range of 2.0 to 4.0 mg-Cr/kg. The conventional methods of removing toxic Cr(VI) which includes the use of inorganic reductants are generally not preferred industrially due to their unavoidable environment unfriendly and cost ineffective nature. Therefore, in this study the use of *Terminalia chebula*, which is a naturally occurring organic product, is explored for Cr(VI) removal in chromite concentrates. The parameters in critical Cr(VI) removal process such as *Terminalia chebula* dosages, contact time and water requirements for application of this method are estimated and used at plant scale. It was found that 540 g of *Terminalia chebula* and contact time of 120 s is required for one ton concentrate treatment at plant for minimizing Cr(VI) to trace levels of 0.02 mg-Cr/kg. It was also observed that the water requirements in using *Terminalia chebula* method are insignificant. The application of *Terminalia chebula* for removing Cr(VI) in chromite concentrate is found to be suitable method for using in continuous production process of chromite concentrates at plant.

(cf. *ISIJ Int.*, **48** (2008), 868)